



# Enhancing performance of phosphorus containing vanillin-based epoxy resins by P–N non-covalently functionalized graphene oxide nanofillers

Pitchaimari Gnanasekar<sup>a</sup>, Heyu Chen<sup>a</sup>, Nicole Tratnik<sup>b</sup>, Martin Feng<sup>c</sup>, Ning Yan<sup>a,b,\*</sup>

<sup>a</sup> University of Toronto, Department of Chemical Engineering and Applied Chemistry, 200 College Street, Toronto, ON M5S 3E5, Canada

<sup>b</sup> Institute of Forestry and Conservation, University of Toronto, 33 Willcocks Street, Toronto, ON, M5S 3B3, Canada

<sup>c</sup> Wood Products Division, FP Innovations, 2665 East Mall, Vancouver, BC, V6T 1W5, Canada

## ARTICLE INFO

### Keywords:

Vanillin epoxy  
Flame retardancy  
FGO  
Thermal properties  
Cone calorimetry

## ABSTRACT

In this study, non-covalently functionalized graphene oxide (FGO) containing phosphorus and nitrogen was synthesized using dibenzyl *N,N'*-diethyl phosphoramidite (DDP) via a single step process. Meanwhile, novel bio-based phosphorus containing vanillin epoxy resin (VPE) was made via a two-step process and used as a flame-retardant adhesive. Subsequently, FGO was dispersed in the epoxy resin matrix at different weight ratios as reinforcement for improving mechanical, thermal and flame-retardant properties of the resultant composite systems. Curing behavior of the VPE and FGO mixtures with 4,4'-diaminodiphenylsulfone (DDS) as the cross-linker was investigated using a Differential Scanning Calorimeter (DSC). Thermal and flame-retardant properties of the cured VPE/FGO nanocomposites were systematically investigated by Thermogravimetric Analysis (TGA), Gas Chromatography – Mass Spectrometry (GC-MS), Limited Oxygen Index (LOI), vertical burning test (UL-94), and cone calorimeter test. Results indicated that all VPE/FGO nanocomposites exhibited excellent thermal and flame-retardant properties. In particular, VPE with 9 wt% of FGO achieved the highest LOI value (29.1%) and passed the V-0 rating in the UL-94 test. Furthermore, cone calorimetry test showed that flame retardancy performance of the VPE and VPE/FGO composites significantly improved compared to vanillin epoxy control resin without phosphorus. The gaseous and high boiling pyrolysis products of VPE cured by DDS were collected and characterized by GC/MS to reveal their formation mechanisms. The char layers of the cured VPE showed a high oxidation resistance with intumescent structures. The combined barrier and quenching effects of the char layer imparted VPE with excellent flame retardancy. This study illustrated a promising approach for synthesizing mechanically strong, thermally-stable and environmentally-friendly flame-retardant bio-based composite resins.

## 1. Introduction

Nowadays, about 80% of commercially available epoxy resins are produced via the reaction between diglycidyl ether of bisphenol A (DGEBA) and epichlorohydrin in alkaline mediums [1]. It is well known that DGEBA is a toxic material, which can have a substantial negative impact on human health and the environment. As a result, there are growing efforts to develop new synthetic methods that can use bio-based alternatives to DGEBA [1–3] with less toxicity. DGEBA epoxy resins have been widely used in many fields, such as composites, coatings, adhesives, laminates, and electronic packaging materials [4]. However, epoxy resins are flammable, which limits their applications when high thermal stability and flame retardancy are required [5–7]. Traditional halogenated flame retardants are undesirable, and their usage is phasing

out since they release toxic gases and other potentially dangerous halogenated compounds during combustion [8].

Recently, bio-based compounds have attracted strong interests as feedstock for polymer synthesis due to increased environmental concerns and potential economic benefits. It has been shown that some polymeric resins can be made from a wide variety of biomass resources and biomolecules, such as vegetable oils, rosin, cardanol, lignin etc., with a lower cost and higher environmental benefits [9–11]. Previous studies have successfully synthesized bio-based epoxy resins as alternatives to petroleum-derived counterparts [12–15]. However, there are limitations associated with these bio-based epoxy resins, such as poor performance due to the presence of long flexible aliphatic chains and low reactivity of the internal epoxy functional groups [16]. Vanillin, a non-toxic mono aromatic biomolecule, can be produced from lignin on

\* Corresponding author. University of Toronto, Department of Chemical Engineering and Applied Chemistry, 200 College Street, Toronto, ON M5S 3E5, Canada.  
E-mail address: [ning.yan@utoronto.ca](mailto:ning.yan@utoronto.ca) (N. Yan).

an industrial scale. Moreover, vanillin has been explored previously as a renewable building block for making bio-based polymers [17,18]. But the synthesis of di-functional epoxies from vanillin is challenging, because only one –OH functional group is available for introducing the oxirane group. In general, either oxidation or reduction of vanillin's aldehyde functional group is needed to create two suitable –OH groups enabling the generation of two epoxy moieties. These reaction pathways are quite complex and use toxic compounds in order to add difunctional phenolic OH groups on the vanillin molecule. To overcome the complexity and avoid the usage of toxic compounds, in this work, we used an organophosphorus oligomer, diphenyl phosphine oxide (DPO), to react with vanillin to obtain difunctional phenolic OH groups on vanillin, which, then, reacted with epichlorohydrin to produce a vanillin-based phosphorus containing difunctional epoxy resin [19].

There is an increased interest in developing phosphorus (P) containing epoxy resins for a higher flame retardancy. Most phosphorus-containing epoxy systems have shown a decrease in their glass transition temperatures ( $T_g$ ) compared to the phosphorus-free systems [20], with fewer literature [21] work reporting a higher  $T_g$  for the P containing epoxy systems. The glass transition temperature of a thermosetting polymer is closely related to the stiffness of its backbone and the level of crosslinking of the polymer network. With the rising desire for utilizing green chemistry approaches to lower environmental impact, there are growing efforts in using renewable resources as the feedstock to synthesize bio-based epoxy resins [21,22]. Hence, in this study, we developed a novel method to use vanillin as the starting material for making thermally-stable and flame-retardant bio-based epoxy resins by skeletally incorporating a phosphorus containing organic compound into the backbone of the vanillin epoxy.

Graphene oxide has been used as a flame-retardant additive in polymer nanocomposites with good results [23,24]. However, graphene is easily burnt out upon exposure to heat in air, which could reduce its effectiveness as a barrier to prevent the escape of organic volatiles in the polymer nanocomposites. To solve this issue, chemical modification of graphene by flame-retardant molecules has been pursued by researchers [25,26]. Generally, efforts on chemical modifications of graphene oxide (GO) have focused on two main strategies, covalent or non-covalent functionalization, to improve the dispersion and compatibility of graphene or graphene-based materials in polymer matrices [27]. When compared to chemical modifications via covalent bonding between graphene oxide (GO) and flame-retardant (FR) compounds, non-covalent bonding of GO with FR has several advantages, such as high efficiency and easy synthesis. One key advantage of non-covalent functionalization through  $\pi$ - $\pi$  interactions is that it does not change the original physical and chemical properties of GO. Previous study showed that, functionalized graphene oxide (FGO) has a higher compatibility with the polymer matrix, i.e. better dispersion, and an enhanced charring capacity [28]. Among various compounds used to functionalize graphene, phosphorus- and/or nitrogen-containing compounds were highly attractive due to their eco-friendly characteristics and strong catalytic carbonization effects during combustion [29].

In this research work, we first synthesized novel high-performance flame-retardant phosphorus containing bio-based epoxy resin (VPE) from vanillin using a recently developed novel synthesis method [30, 31]. Then, the functionalization of graphene oxide (FGO) was prepared through non-covalent  $\pi$ - $\pi$  stacking interactions with a flame-retardant compound, dibenzyl *N,N*-diethyl phosphoramidite (DDP), containing both phosphorus and nitrogen elements. Afterwards, the FGO was directly blended with VPE epoxy in different weight fractions. The epoxy network was obtained by epoxy curing via ring opening reactions with 4, 4'-diaminodiphenylsulfone (DDS) as the curing agent. The curing kinetics, thermal, mechanical, and bonding properties, and combustion behavior of control vanillin epoxy resin without phosphorus (VE), VPE resin, and VPE/FGO nanocomposites systems were investigated by Thermogravimetric Analysis (TGA) and cone calorimetry, and the relevant flame retarding mechanisms were discussed. Results showed that

thermal stability and lap shear bonding strength of the cured VPE resin systems were all simultaneously improved compared to VE control. The goal of this research was to develop a flame-retardant bio-based epoxy composite system with potential to replace DGEBA based epoxy resins for applications requiring high flame retardancy performances.

## 2. Experimental

### 2.1. Preparation of GO and FGO

In this study, the modified hummers method was used for the preparation of graphene oxide (GO) from graphite [32,33]. The oxidation reactions of graphite can efficiently condense the van der Waals forces between the nearby carbon sheets, and the water molecules can readily penetrate the interlayers of GO. Therefore, with the assistance of mild sonication, the GO can be exfoliated into single-layer nanosheets in water. Afterwards, 20 mL of alcoholic solution of Dibenzyl *N,N*-diethyl phosphoramidite (DDP) (150 mg) was added dropwise into the GO suspension under a constant stirring. Due to the difference between the polarization of water and ethanol, DDP became less soluble in water. Hence, the less soluble DDP was attached to GO via strong  $\pi$ - $\pi$  interactions. Continuous penetration of DDP molecules into the GO sheets helped to achieve a more stable dispersion of FGO in water [34]. Then, the supernatant liquid was decanted, and the residuals were then rewashed again with HCl and deionized water for 5 times. The washed FGO sample was dried using an oven set at 90 °C for 24 h to produce FGO powders. The preparation procedure of flame-retardant FGO is illustrated in Scheme 1.

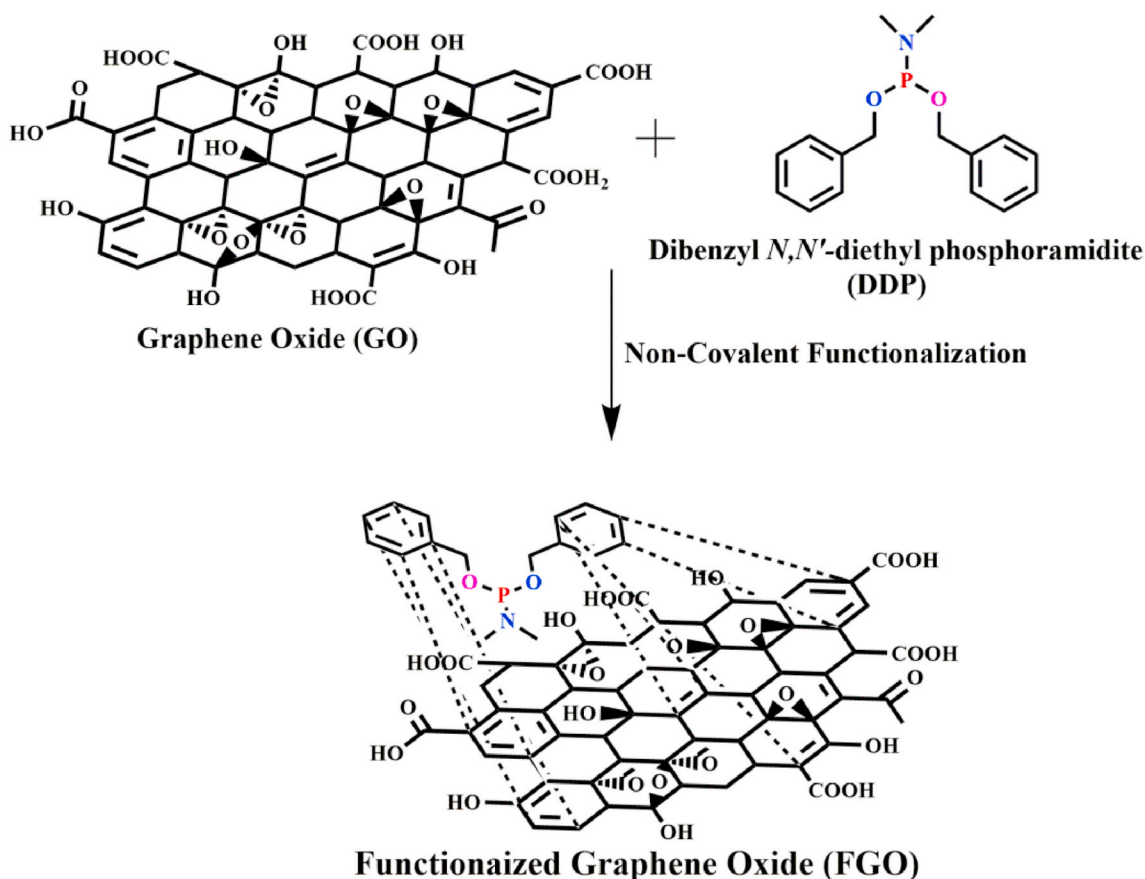
### 2.2. Preparation of VPE/FGO composite resins

Different weight fractions of FGO was added to ethanol and sonicated until the suspension became clear with no visible particulate matter. The suspension was mixed with the VPE resin and sonicated for 1.5 h. Afterwards, the ethanol solvent was evaporated by heating the mixture on a magnetic stir plate using a Teflon-coated magnetic bar for 3 h at 70 °C. Furthermore, the FGO/VPE mixture was placed in a vacuum oven for 24 h at 70 °C to ensure that all ethanol had been removed. Then, the mixture was placed in an oil bath at 90 °C and a stoichiometric amount of curing agent, diamino diphenylsulfone (DDS), was slowly added, under continuous mechanical stirring, until the solution became a homogeneous mixture. Several DSC aluminum pans were filled with the reaction mixture. The samples (~10 mg) were then cooled and stored in a freezer until required. The weight fractions of FGOs in the VPE/DDS system were 3, 5, 7 and 9 wt %, and were labeled as VPE/3% FGO, VPE/5%FGO, VPE/7%FGO, and VPE/9%FGO, respectively.

## 3. Results and discussion

### 3.1. FTIR analysis

FTIR spectra confirming the molecular structure of the synthesized phosphorus containing vanillin (VP), phosphorus-vanillin based epoxy resin (VPE), control vanillin epoxy without phosphorus (VE), graphene oxide (GO), functionalized graphene oxide (FGO) and VPE/FGO nanocomposites are shown in Fig. 1. FTIR measurement was carried out in wavelengths of 4000–400  $\text{cm}^{-1}$ . The FTIR spectrum of DPO showed the presence of an absorption peak at 2352  $\text{cm}^{-1}$  attributed to P–H group [35]. The absence of the absorption peak at 2352  $\text{cm}^{-1}$  and the strong peak noted at 3425  $\text{cm}^{-1}$  in the FTIR spectrum were attributed to the OH group formation in VP indicating that the reaction occurred between DPO and Vanillin [31,35]. The FTIR spectrum of phosphorus containing vanillin-based epoxy resin (VPE) is also shown in Fig. 1. The most evident functional group of this compound is the oxirane which has an absorption peak at 918  $\text{cm}^{-1}$ , confirming the formation of epoxide rings. The peaks appeared at 2875  $\text{cm}^{-1}$  and 1657  $\text{cm}^{-1}$  represented the



Scheme 1. Schematic illustration for the preparation of functionalized graphene oxide (FGO).

aliphatic and aromatic  $-\text{CH}_2$  groups, respectively [36].

In the FTIR spectra, the presence of phosphorus in the VPE backbone was confirmed by the characteristic absorption peaks at  $3446(\text{O-H})$ ,  $1429(\text{Ph})$ ,  $1130(\text{P=O})$ ,  $733$  and  $711\text{ cm}^{-1}(\text{P-Ph})$  [37], and the absence of the distinctive absorption at  $2352\text{ cm}^{-1}$  for  $\text{P}(\text{O})-\text{H}$  that was present in neat DPO. Functionalization of the flame-retardant group on GO was also confirmed by the FTIR spectrum. The FTIR spectrum of GO showed some typical absorption peaks of oxygen-containing groups:  $\text{O-H}$  stretching vibration ( $3418\text{ cm}^{-1}$ ),  $\text{C=O}$  stretching vibration ( $1732\text{ cm}^{-1}$ ),  $\text{C=C}$  or  $\text{H}_2\text{O}$  vibration ( $1625\text{ cm}^{-1}$ ), and  $\text{C-O}$  stretching vibration ( $1230\text{ cm}^{-1}$ ) [38]. After being functionalized by DDP, a slightly decreased intensity for the peak at  $3418\text{ cm}^{-1}$  was observed in the spectrum of FGO, suggesting that functionalization of GO by DDP mostly occurred by non-covalent strategy [39]. Additionally, the distinctive absorption peaks for  $\text{P-N}$  stretching appeared at  $1085\text{ cm}^{-1}$  [40]. FTIR spectra for thermally cured neat VE, VPE, VPE/FGO nanocomposites were shown in Fig. S4. (Supporting Information). It could be seen that the peak at  $918\text{ cm}^{-1}$  was nearly absent in all cured systems, indicating the successful opening of the oxirane ring upon the curing reactions. The opening of the oxirane ring was further supported by the broadened peak noted at  $3500\text{ cm}^{-1}$ , which corresponded to the formation of hydroxyl groups during the ring opening polymerization.

### 3.2. DSC studies of the uncured VPE resins and cured VPE/FGO composites

The dynamic DSC curves recorded at the heating rate ( $\beta$ ) =  $20\text{ }^\circ\text{C}/\text{min}$  for the neat VE, VPE and VPE/FGO nanocomposites are shown in Fig. 2(a). It was clear that VPE and VPE/FGO nanocomposites underwent oxirane ring opening polymerization without phase transformation. The DSC curves of neat VE and VPE/3%GO at different

heating rates,  $\beta$ , ( $10$ ,  $20$ , and  $30\text{ }^\circ\text{C}/\text{min}$ ) are shown in Fig. S5 (A) and (B) (Supporting Information), respectively. The parameters, such as onset temperature ( $T_S$ ), end set temperature ( $T_E$ ), maximum curing temperature ( $T_{MAX}$ ), and enthalpy of curing ( $\Delta H_C$ ), derived from the DSC traces recorded at different  $\beta$  values for VPE and FGO nanocomposites are presented in Table S1 (Supporting Information). As shown in Fig. 2(a), the addition of FGO clearly decreased the onset and maximum peak temperature ( $T_p$ ) of the curing reactions. This could be caused by reactive hydrogens from the remaining  $-\text{OH}$  and  $-\text{COOH}$  groups on the FGO surfaces accelerating curing reactions in the epoxy-amine systems [41]. When compared to GO, the surface of FGO still had some reactive hydrogens from  $-\text{OH}$  and  $-\text{COOH}$  group at  $3418\text{ cm}^{-1}$  after the functionalization of GO. Obviously, the FGO sample with a high content of hydrogen-containing groups and a good dispersion state could show a higher accelerating effect on the curing reactions. This indicated that FGOs could act as catalysts to promote the curing reaction. The curing enthalpy ( $\Delta H$ ) of the FGO/epoxy nanocomposites was smaller than that of the neat epoxy system. The  $\Delta H$  value decreased from  $135.60\text{ J/g}$  for neat epoxy to  $110.3\text{ J/g}$  for graphene oxide/epoxy nanocomposite with an addition of  $9\text{ wt}\%$  FGO. This indicated that the oxygen functionalities present on the surface of the functionalized graphene oxide (FGO) acted as catalysts to accelerate the curing reaction between the epoxide and the amine groups [42].

The glass transition temperatures ( $T_g$ ) of the cured VE, VPE and VPE/FGO nanocomposites are shown in Fig. 2(b) the  $T_g$  values of the VPE/FGO nanocomposites were slightly shifted to a lower temperature when compared to those of the neat VE and VPE. This decrease could be due to two reasons. First, FGO could interfere with the curing of epoxy by unbalancing the stoichiometry of the curing reaction, resulting in less cross-linking. Second, a larger amount of the solvent was required to disperse the higher loadings of FGO, which also needed a prolonged

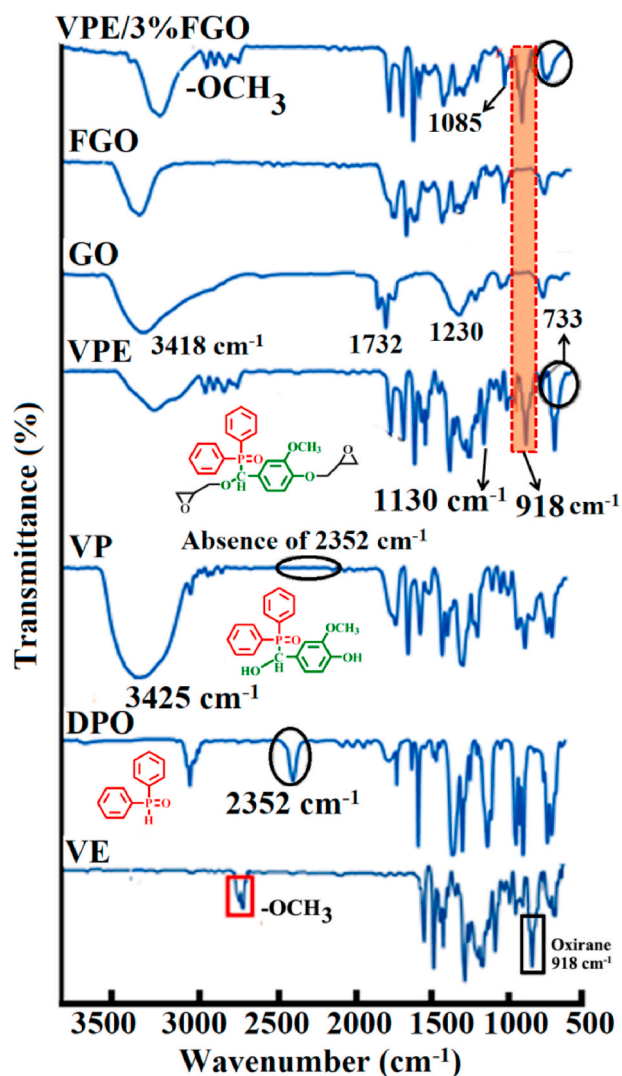


Fig. 1. FTIR spectra of the synthesized VE resin, VP, VPE resin, GO, FGO, and VPE/3%FGO resin composite.

heating to evaporate the solvent completely. As a result, the possibility of reactions between the solvent and epoxy could not be ruled out, which would also reduce the degree of cross-linking. Similarly, several previous studies of graphene containing epoxy composites reported the shifting of  $T_g$  towards lower temperatures [43,44]. A lower  $T_g$  was attributed to the increase in free volume which rendered easier

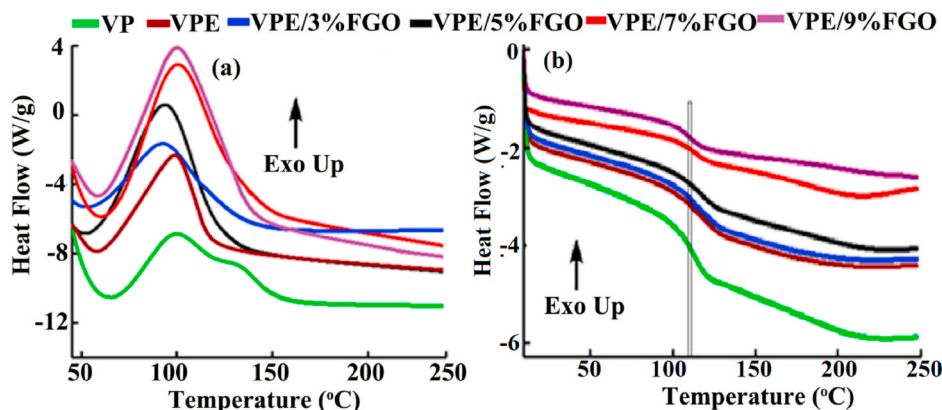


Fig. 2. (a) DSC curing curves and (b)  $T_g$  measurement traces of VE, VPE and VPE/FGO nanocomposites at the heating rate ( $\beta$ ) = 20 °C/min.

movement of the uncured epoxy and the entrapment of the residual solvent in the polymer matrix [43].

### 3.3. Effects of FGO on curing kinetics

Fig. 3 plots activation energy ( $E_a$ ) versus reaction extent ( $\alpha$ ) for the neat VPE resin and VPE/FGO nanocomposites. The values of  $E_a$  for VPE was relatively lower at  $\alpha = 0.1$  when compared to that of VPE/FGO nanocomposites except for VPE/3%FGO. For VPE,  $E_a$  values increased steadily with the increase in the reaction extent from  $\alpha = 0.1$  to 0.55. After  $\alpha$  reached 0.6, the  $E_a$  values increased sharply until the end of the reaction. A similar behavior was noted for the VPE/3% FGO sample, but with slightly lower  $E_a$  values than those of neat VPE. Thus, even at the lowest level (3%) of FGO addition, the curing reaction of VPE was affected by the presence of FGO. The trend for VPE/5%FGO, VPE/7% FGO, and VPE/9%FGO nanocomposites was different. At the initial stage of the reaction, i.e.  $\alpha = 0.1$ , a higher  $E_a$  value was noted for VPE/5%FGO, VPE/7%FGO and VPE/9%FGO when compared to neat VPE. For these three types of nanocomposites, the  $E_a$  values were gradually decreased when  $\alpha$  increased from 0.1 to 0.35. The decline in  $E_a$  values was mainly attributed to the autocatalytic curing reaction through epoxide ring opening initiated by FGO. This observation was reported previously by studying the curing kinetics of epoxy/graphene oxide (GO) nanocomposites [45]. When  $\alpha$  became higher than 0.4, the  $E_a$  values gradually increased until the end of the curing reaction, which corresponded with the progress of the epoxy ring opening reaction at

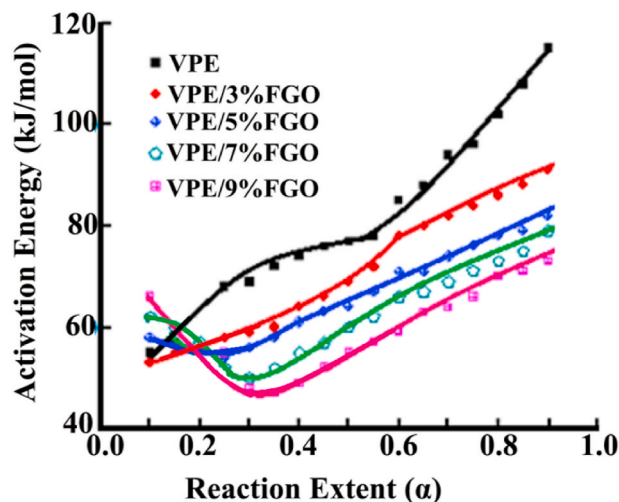


Fig. 3. Relationship between reaction extent and activation energies during the curing reactions of neat VPE and VPE/FGO nanocomposites resin systems.

different stages of the curing process. The rise of  $E_a$  at the higher reaction extent ( $\alpha = 0.4-0.9$ ) was probably due to the increase in the cross-linking density of the chemical structure, leading to more constraints on the movement of the molecular segments in the curing process to result in the increase in the activation energy.

Based on the previous findings [46], the ring opening polymerization reaction mechanisms for the neat epoxy resins (VPE) in curing was proposed in Scheme 2. In the initial stage of curing, primary amine group present in DDS opened the epoxy ring leading to the generation of secondary amine and hydroxyl groups. The generated secondary amine caused the formation of tertiary amine with a rise in hydroxyl groups. Lastly, the hydroxyl groups led to the formation of branched ether linkages. A similar reaction mechanism can be expected for VPE/FGO nanocomposites. For VPE/FGO systems, the cure initiation reaction was slightly hindered due to the presence of carboxylic acid groups present in FGO, which neutralized the basic amine groups of the hardener to result in the formation of amide linkages during the curing reaction, thereby leading to higher activation energies at the initial degree of conversions ( $\alpha$ ), when compared to the neat epoxy system (VPE).

As the curing reaction proceeded, the autocatalytic effect of FGO on VPE took place as what is shown in Scheme 3. It involved both addition and etherification reactions. As represented in Scheme 3, carboxyl (or hydroxyl) groups on FGO formed hydrogen bonding with VPE, followed by the formation of a VPE-FGO-DDS trimolecular transitional complex. The complex formation proceeded with further epoxide ring openings. Subsequently, secondary amine from DDS was formed after fast proton transfer. The resultant secondary amine could react with the remaining VPE in a similar manner to FGO showing an autocatalytic effect. Moreover, there was another possibility that the tertiary amine present in the FGO as part of the DDP molecule could also serve as a catalyst to accelerate the curing reactions between the epoxide and the amine groups. Jouyandeh et al. [47], showed that the major functionalities present in FGOs were ketones, six membered lactol rings, tertiary alcohol, and epoxide and hydroxyl groups. Clearly, the oxygen functionalities present on the surface of FGOs catalyzed the curing reaction between the VPE epoxide and DDS amine groups.

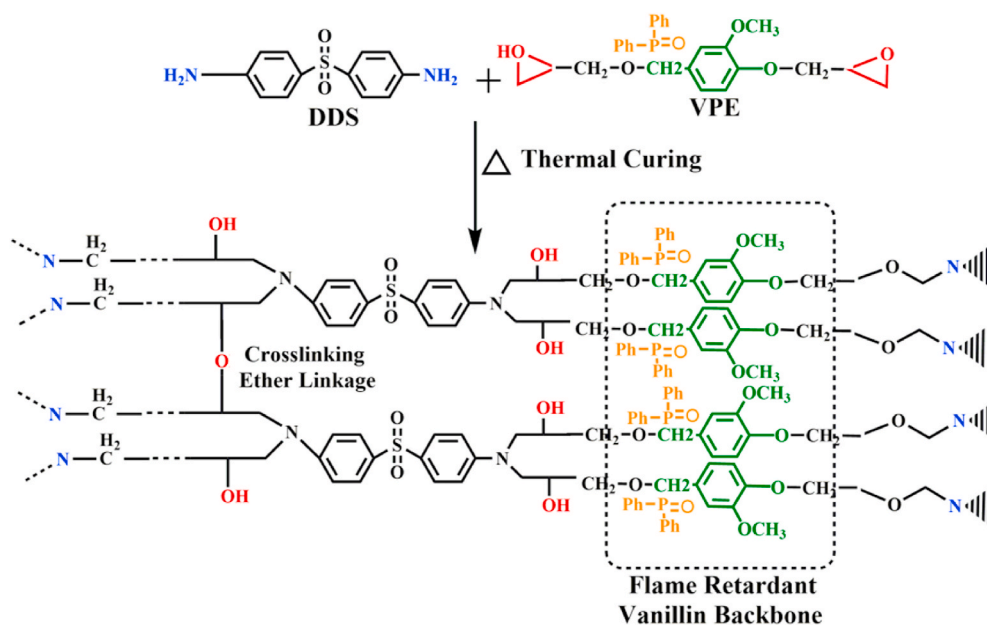
### 3.4. Raman Spectra analysis

Raman spectrum analysis was used to exam the level of dispersion of FGO in the VPE matrix. The characteristic Raman spectra obtained from

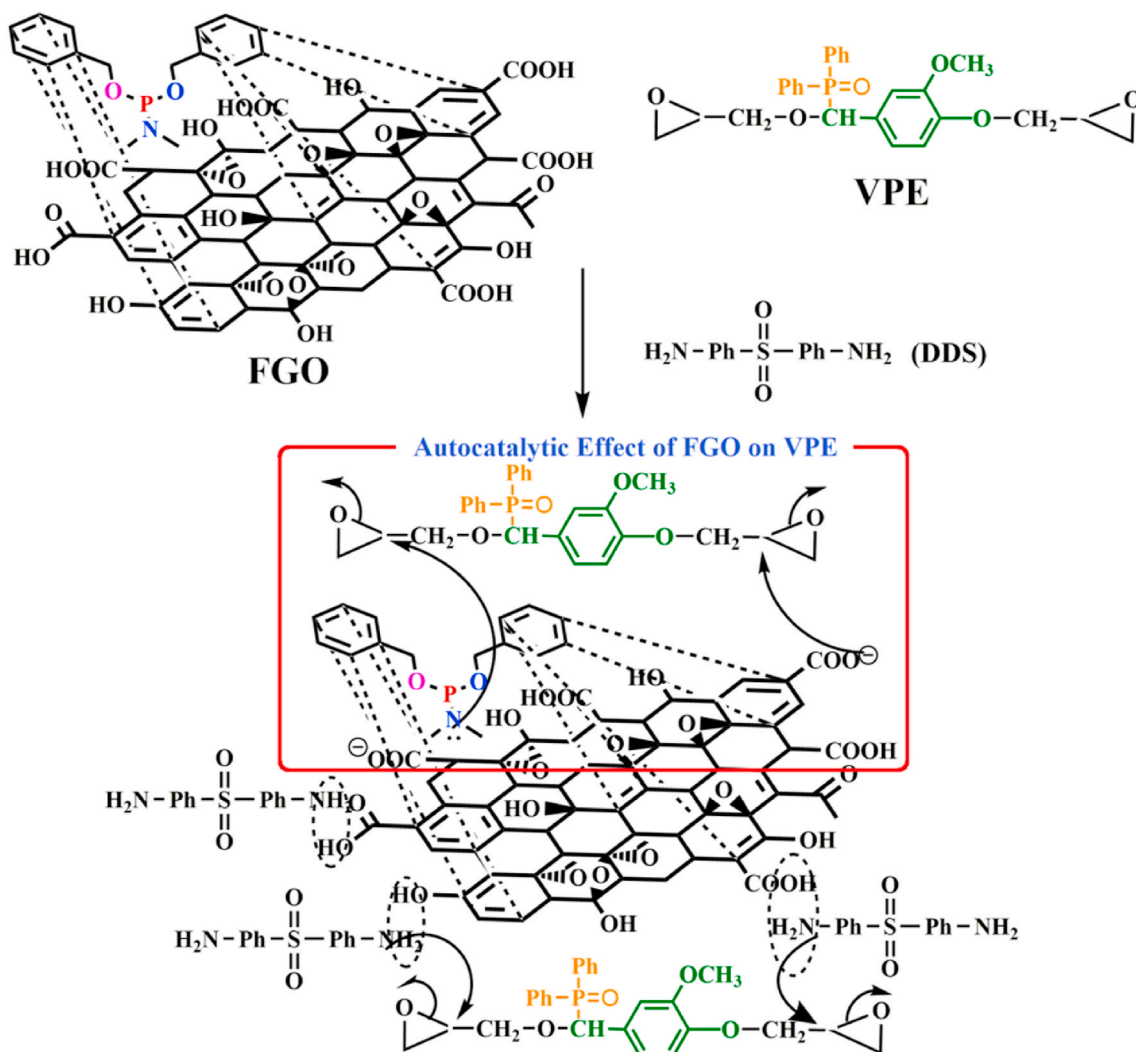
GO, FGO, and epoxy are shown in Fig. 4 (A). The bulk GO showed two intense bands clearly displayed at  $1585\text{ cm}^{-1}$  (G band), corresponding to the n-plane stretching motion of symmetric  $\text{sp}^2$  C-C bond, and at  $1381\text{ cm}^{-1}$  (D band), indicating the presence of defects inherent in the edge effect of A1g vibration mode. The above observations confirmed the significant structural changes occurred during the oxidization of graphite to GOs [48]. Compared to GO, the G band of FGO and VPE/FGO nanocomposites shifted to a higher frequency which could be attributed to the distortion of the double bonds and the reduction of symmetry due to the decrease of the size of the E2g vibrational mode of  $\text{sp}^2$ -bonded ( $\pi$  bond) graphitic carbon. These explanations were supported by previous results [49]. Moreover, the D band showed a relatively higher intensity which was consistent with the  $I_D/I_G$  ratio changing from 0.94 to 1.01 for GO and FGO, respectively (Fig. 4(A)). The increased intensity ratio of  $I_D/I_G$  was due to the formation of more  $\text{sp}^3$  domains ( $\sigma$  bond). The increased  $I_D/I_G$  ratio of FGO (1.01) as compared to GO (0.94) was caused by the free radical functionalization of the  $\pi$  bond present in the GO sheets. The intensity of D band for VPE/FGO was directly proportional to the level of imperfection (i.e. different levels of formation of  $\text{sp}^3$  domains in FGO) in the sample and represented the degree of functionalization when GO was chemically modified. A similar observation was made by previous researchers that the intensity of D bands of epoxy with GO was higher than that of GO alone [50].

### 3.5. XRD analysis

The XRD analysis was carried out for GO, FGO, VPE, and VPE reinforced with different weight percentages of FGO and the results are shown in Fig. 4(B). The typical diffraction peak at  $2\theta = 12.1^\circ$  of GO was the 002 reflection peak, which was equivalent to an interlayer spacing of about  $0.34\text{ nm}$  [51]. When compared to GO, FGO only had a weak diffraction peak at  $2\theta = 33.2^\circ$ , confirming a larger interlayer spacing ( $0.93\text{ nm}$ ) in FGO. It might be the result of the remaining functional groups presented on the GO surfaces that facilitated dispersion [52]. However, there was a shift in the peak intensity of FGO filled VPE epoxy nanocomposites from  $2\theta = 32.4^\circ$  for FGO to  $2\theta = 23.3^\circ$  for the composites. The intensity of the peaks at this  $2\theta$  increased significantly with an increasing amount of FGO. The shift of the intensity peak towards a lower angle indicated that the interplanar spacing among the graphite platelets of FGO decreased, suggesting that there was mixed intercalated and exfoliated FGO platelets in the epoxy nanocomposites [38,39], The



Scheme 2. The proposed curing process between VPE and DDS.



Scheme 3. Schematic illustration of VPE-FGO-DDS trimolecular transition complex.

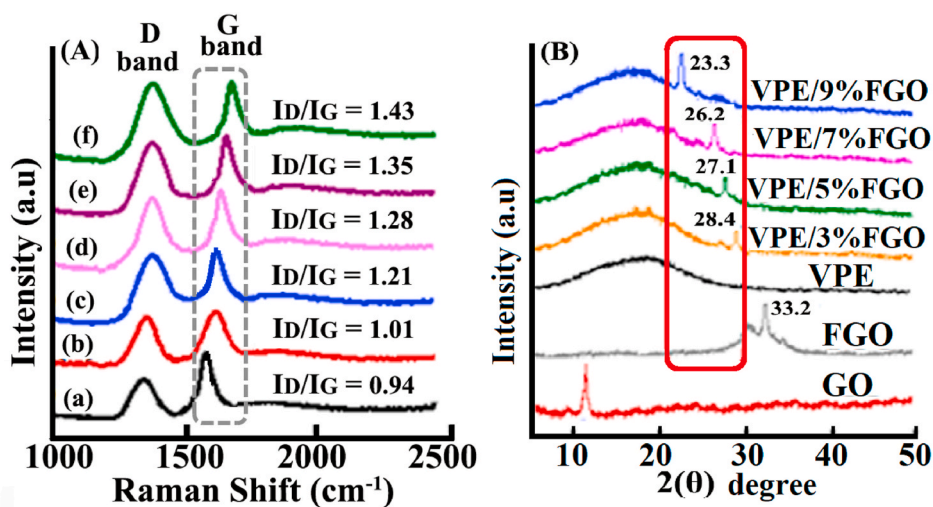


Fig. 4. (A) Raman Spectra of (a) GO, (b) FGO, (c) VPE/3%FGO, (d) VPE/5%FGO, (e) VPE/7%FGO, (f) VPE/9%FGO. (B) XRD spectra of GO, FGO, neat VPE, and VPE/FGO nanocomposites.

decrease in the interplanar spacing was higher with a higher FGO content in the system, implying that the systems with a lower level of FGO loading had more exfoliated morphologies. When compared to VPE/FGO, the neat VPE epoxy resin demonstrated a broad diffraction peak centered at  $2\theta \approx 20^\circ$  originated from the scattering of the cured epoxy network, indicating the amorphous nature of the polymer. It could be seen that all VPE/FGO composites showed a similar diffraction pattern, due to the homogenous dispersion and complete exfoliation of FGO in the VPE epoxy matrix. Therefore, these results clearly indicated that non-covalent bonding between VPE and FGO had resulted in significant structural changes in the carbon lattice.

### 3.6. Scanning electron microscope analysis

Surface morphology of GO and FGO and the dispersion of FGO in VPE were characterized by the SEM analysis. Fig. S7 (a) and (b) (Supporting Information) illustrated the morphological characteristics of GO and FGO, respectively. In Fig. S7(b), the surface of FGO had a higher roughness compared to that of GO [53]. The EDX mapping in Fig. S7 (b) showed intense signals of C, N, P and O for FGO confirming the functionalization. The absence of other elemental signal indicated the high purity of FGO, which was achieved by repeated cycles of water and methanol washes to remove any unwanted ions [54]. Due to the good affinity of  $H^+$  and  $Cl^-$  ions towards water, these ions were removed from the prepared FGO during washing.

The level of dispersion of FGO in the epoxy matrix was also examined by SEM and shown in Fig. S7 (c-f). In Fig. S7(c), the surface morphology of VPE was considerably smoother than that of the VPE/FGO nanocomposites. Fig S7 (d-f) clearly showed that the roughness of the surfaces of the VPE/FGO nanocomposites drastically increased upon the addition of FGO due to the dispersion of the graphene sheets throughout the matrix [55]. In addition, FGO were well exfoliated with little visible agglomerates. It also showed that the homogeneously dispersed FGO were strongly bonded with the epoxy matrix without any debonding or pull-out of the FGO nanolayers. The strong bonding could be the result of covalent bond formation between the epoxy matrix and FGO sheets during the curing process. Improved dispersion and bonding of the FGO sheets would significantly enhance the final mechanical properties of the composites [56].

### 3.7. Bonding properties

The average lap shear bonding strengths (dry strength, cold water treatment, and boiling water treatment) of the neat epoxy and their VPE/FGO nanocomposites are shown in Fig. 5. It clearly showed that the lap shear bonding strength increased with the addition of FGO up to 7 wt% level. There was a slight drop in the lap shear bonding strength with 9 wt% of FGO. Therefore, an optimum existed for the addition amount of FGO in order to maximize the bonding properties. It had been suggested by previous studies that the viscosity of the epoxy resin would increase with the increasing percentages of FGO [57]. Since both smaller contact angles and increasing viscosity were associated with a less degree of penetration by the uncured liquid resin according to the Washburn equation, it could be concluded that with higher loadings of FGO (after 7% FGO) epoxy resin did not penetrate as much as the case when lower amounts of FGO were added.

Results from the failure mode analysis of the lap shear test specimens further supported the trend observed for the lap shear bonding results. The cold water-soak test method required the wood specimen to be dried (after soaking) prior to the testing, but in the case of boiling water treatment the specimen was tested in the wet state. As a result, failure mode for dry strength test and cold water soaked and dried specimens were wood substrate failure. However, the boiling water-soaked specimen's failure mode was mostly by failure in the adhesive layer. The bonding strength for dry and cold-water soaking test was limited by the cohesive strength of the wood substrate itself [58]. Overall, FGO

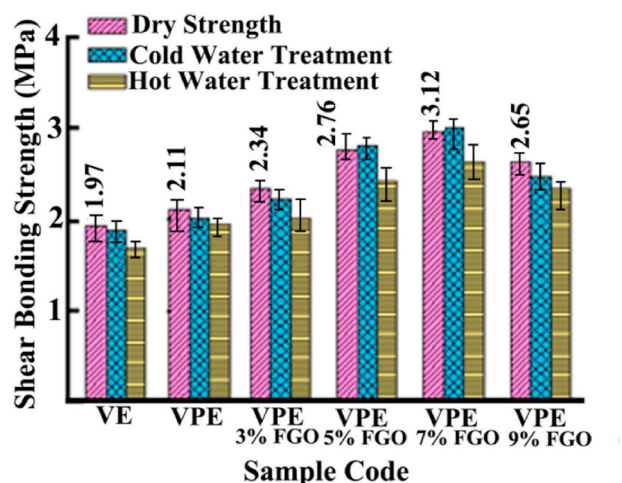


Fig. 5. Average lap shear bonding strength for neat VE, VPE and VPE/FGO nanocomposites under different test conditions.

enhanced the lap shear bonding strength of the neat resin systems and the composite showed a higher resistance to water penetration.

### 3.8. Thermal degradation and flame retardancy studies

TGA studies were performed to evaluate the thermal degradation properties of the neat VPE and FGO/VPE nanocomposites. The TG and DTG curves for GO, FGO and thermally cured VE, VPE, and VPE/FGO nanocomposites are shown in Fig. 6. The onset ( $T_S$ ), maximum ( $T_{MAX}$ ), and endset ( $T_E$ ) temperatures of thermal degradation and the amount of char residue obtained at 600 °C for all samples are tabulated in Table S2 (Supporting Information).

Fig. 6 showed that neat VE underwent a single stage thermal degradation process in the temperature range of 250–380 °C, which was due to thermal degradation of neat VE polymer network. Meanwhile, DTG curve of thermally cured VPE showed multistage degradations overlapping with each other, indicating that the second thermal degradation process of VPE started before the completion of the first degradation process. Incorporation of FGO had no effect on the overlapping nature of the degradation stages of the cured VPE, but the thermal degradation onset temperature shifted toward lower temperatures compared to those of neat VPE, which was attributed to the increase of labile oxygen functional groups on the surface of FGO. However, the char value was increased after the addition of FGO, which was due to the flame-retardant groups grafted on FGO promoted the char formation. Therefore, the increase in char residue could form a barrier to protect the nanocomposites from further oxidative degradation.

In general, the initial stage of thermal degradation of phosphorus-nitrogen containing FGO additives could catalyze the degradation of polymers to form a shielding char layer. The char yield at 600 °C, i.e. the residue percentage, of pure VPE was approximately 20.3%. VPE/9% FGO samples exhibited the highest char residues (24.1% @ 600 °C) than other FGO addition levels (3, 5 and 7 wt%) indicating that the catalytic charring effect of P-N groups present in the FGO was the main reason. The formation of high char residues during combustion decreased the release of combustible gases and inhibited the mass and heat transfer between the condensed phase and the gaseous phase, thus slowing down the heat release rate [59,60]. Besides, the char layer could shield polymers from flame in the early stage of ignition [61]. Hence, even though FGO reduced thermal stability in the initial stages, the char residue increased with an increasing FGO content up to 24.1% @ 600 °C (Table S2, (Supporting Information)).

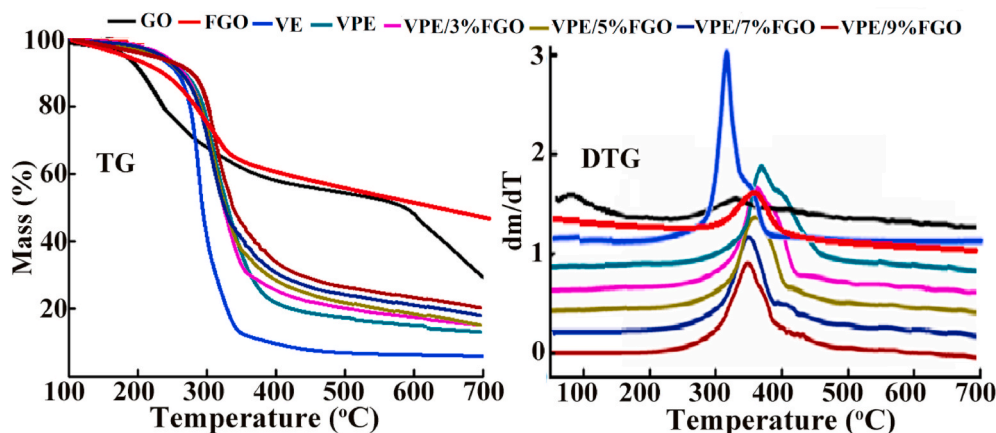


Fig. 6. TG and DTG curves of GO, FGO, and thermally cured VE, VPE, and VPE/FGO nanocomposites.

### 3.8.1. GC-MS studies

In order to investigate the flame-retardant mechanism, decomposition products obtained from VPE during combustion were studied by the GC-MS technique. The mass spectra corresponding to the GC peaks are presented in Fig. 7. The mass spectra of the corresponding GC graph for VPE and DDS clearly showed a new strong peak at 367 m/z corresponding to  $C_{21}H_{20}O_4P$  (VP). Also, peaks at 154 m/z (for  $C_8H_{10}O_3$ ), 107 m/z (for  $C_7H_7O$ ), 201 m/z (for  $C_{12}H_{10}PO$ ) and 120 m/z (for  $C_6HPO$ ) could be assigned to the fragment ions that mainly originated from the degradation of the DPO segment present [31] in VPE shown in Table 1. As well as some other strong peaks at 304 m/z (for  $C_{16}H_{20}N_2SO_2$ ), 235 m/z (for  $C_{12}H_{13}N_2SO_2$ ), 140 m/z (for  $C_6H_4SO_2$ ), 166 m/z (for  $C_{12}H_8N$ ),

93 m/z (for  $C_6H_7N$ ) and 78 m/z (for  $C_6H_6N$ ) were indicative of diamino diphenyl sulphone (DDS) curing agent. Moreover, some fragment ions recombined to form new products under high temperature conditions; for instance, the recombination between benzene and aniline generated carbazole (250 m/z), and the carbazole and benzene reconstituted to produce a few polycyclic aromatic hydrocarbons (166 m/z) [62].

Based on the results of volatile fragmentation, the possible degradation mechanisms of the improved flame-retardant properties of the VPE/FGO nanocomposite are presented in Table 1. The proposed char mechanism was clear that the major degradation started with the phosphorus containing DPO segments and mono aromatic structure present in vanillin segments. Hydroxyl groups formed during ring opening of oxirane ring present in VPE were further degraded to form numerous low molecular weight aromatic compounds (Table 1).

The phosphate species degraded from diphenyl phosphine could catalyze the decomposition of the macromolecular network of the VPE/FGO thermosets to generate various fragment ions. Some ions recombined to form polycyclic aromatic hydrocarbons. Moreover, these active phosphorus ions from DPO could be adsorbed on the surface of FGO, and continually propagated on the graphene to serve as the outline for micro char. Such a char layer would lead to high flame retardancy for the VPE/FGO nanocomposites. Generally, the higher char yield could provide a better flame retardancy of the resin, since the formed char residue could serve as a protective layer to inhibit the transport of heat and oxygen and to prevent the resin matrix from further degradation.

### 3.8.2. LOI and UL94 analysis

LOI and UL-94 tests were conducted to investigate the flame-retardant properties of VE, VPE and VPE/FGO nanocomposites. Corresponding data are presented in Table 2. VE was a highly flammable material with a low LOI value (21.4%) and did not achieve any rating in the UL-94 vertical burning test. Due to the phosphorus present in the backbone of VPE, the LOI value of VPE increased to 26.6% and VPE passed V-0 rating in the UL-94 test. Furthermore, The LOI values for VE/3%FGO, VE/5%FGO, VE/7%FGO, and VE/9%FGO were 27.1%, 27.3%, 28.2%, and 29.1%, respectively and all samples achieved a V-0 rating. These results indicated that VPE and VPE/FGO nanocomposites possessed excellent flame retardancy when compared to vanillin epoxy without phosphorus (VE).

The blowing-out effect [63] was noted for the cured VPE and VPE/FGO nanocomposites during the UL-94 test. Such an effect was not observed for the neat VE. In the case of VE, after the first 20s ignition, the VE specimen burned rapidly, and the fire spreaded very fast from the igniting source to the clamping end. The sample continued to combust until the whole sample burnt out obtaining no UL-94 rating. While in the case of VPE and VPE/FGO, fire on the samples was self-quenched after removing the ignition source. In addition, when the igniter was

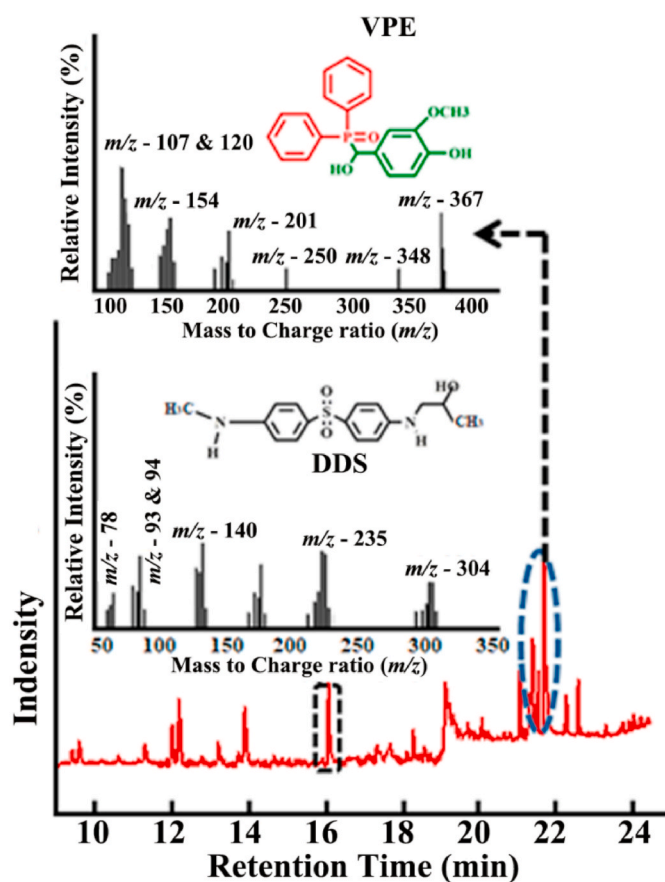
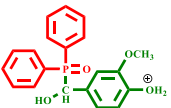
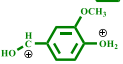
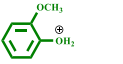
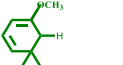
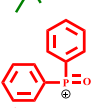
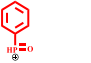
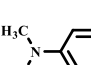
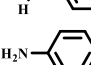
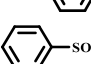
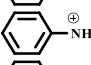
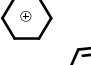
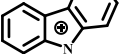


Fig. 7. Gas chromatogram and corresponding mass spectra for the decomposition products of VPE and DDS.



**Table 1**  
Possible mass fragmentation during thermal degradation processes for VPE and DDS backbone.

Sample	Assigned Structure	Molecular Formula	Molecular Weight ( <i>m/z</i> )
Degradation Species Obtained from VPE		C <sub>21</sub> H <sub>20</sub> O <sub>4</sub> P	317
		C <sub>8</sub> H <sub>10</sub> O <sub>3</sub>	154
		C <sub>7</sub> H <sub>6</sub> O <sub>2</sub>	125
		C <sub>7</sub> H <sub>7</sub> O	107
		C <sub>12</sub> H <sub>10</sub> PO	201
Degradation Species Obtained from DDS		C <sub>6</sub> H <sub>8</sub> PO	120
		C <sub>16</sub> H <sub>20</sub> N <sub>2</sub> SO <sub>2</sub>	304
		C <sub>12</sub> H <sub>13</sub> N <sub>2</sub> SO <sub>2</sub>	235
		C <sub>6</sub> H <sub>4</sub> SO <sub>2</sub>	140
		C <sub>6</sub> H <sub>7</sub> N	93
		C <sub>6</sub> H <sub>6</sub>	78
		C <sub>12</sub> H <sub>8</sub> N	166

**Table 2**  
LOI values and UL-94 test results of the cured VE, VPE, and VPE/FGO nanocomposites.

Sample Code	Time to Flame Subjection (S)	Flame after 20 s ignition	Rating	Cotton Ignition	LOI (%)
VE	20	43 s Completely burned	Unrated	N/A	21.4 ± 0.2
VPE	20	9.1 ± 0.5	V0	No	26.6 ± 0.3
VPE/3% FGO	20	9.1 ± 0.3	V0	No	27.1 ± 0.1
VPE/5% FGO	20	8.4 ± 0.4	V0	No	27.3 ± 0.4
VPE/7% FGO	20	7.2 ± 0.3	V0	No	28.2 ± 0.2
VPE/9% FGO	20	6.3 ± 0.2	V0	No	29.1 ± 0.3

removed, the flame was rapidly blown out by the airflows from the igniting end. This was due to the so-called blowing-out effect [64]. The airflows were caused by the jet of pyrolytic gases from the char layer. This phenomenon was also studied by Zhang [65] and Luo et al. [66]. The video screenshots of VE, VPE and VPE/9%FGO during the UL-94 test are shown in Fig. S6 (Supporting Information). The combination of phosphorus and nitrogen atom present in the DDP played a key role in increasing flame retardancy.

### 3.8.3. Cone Calorimetry Testing

Cone Calorimetry Testing (CCT) was conducted to investigate the flame-retardant behavior of the samples. The curves of heat release rate

(HRR), total heat release (THR), and total smoke production rate (TSP) are shown in Fig. 8. Main characteristic fire safety properties, including average heat release rate (*Avg HRR*), peak heat release rate (*Pk HRR*), average CO and CO<sub>2</sub> yield, and average effective heat of combustion (*Avg EHC*) are listed in Table 3.

The HRR curve of the neat VE resin showed a sharp peak and the sample burned very rapidly after ignition and the associated *Pk HRR* and *Avg HRR* THR were 1499.00 kW/m<sup>2</sup> and 144.73 kW/m<sup>2</sup>, respectively. After incorporating phosphorus, the *Avg HRR*, *Pk HRR*, *Avg EHC*, CO yield and CO<sub>2</sub> yield were all decreased. A further reduction in *Avg HRR*, *Pk HRR*, *Avg EHC*, TSP, CO yield and CO<sub>2</sub> yield was also achieved by the addition of FGO and the values for the char residue increased by up to 50%, clearly indicating that a thicker protective char layer formed due to FGO. P–N functional groups on the FGO provided a synergistic mechanism to enhance char formation and reduce thermal conductivity. It was shown in the literature that the P-containing groups could simultaneously act in both the gas phase and the condensed phase (via char formation), while the N-containing groups could release inert gases to dilute oxygen and facilitate the expansion of the char layer during the combustion process [67]. In this study, FGO promoted the formation of an intumescent char layer on the surface of the VPE polymer. The P–N containing intumescent char layer could act as a barrier to inhibit gaseous products and insulate the underlying polymer from heat and air. FTIR analysis of the char residues of the VPE/FGO composites also supported the proposed P–N synergistic flame-retarding mechanism.

*Avg HRR*: Average Heat Release Rate, *Pk HRR*: Peak Heat Release Rate, *Avg EHC*: Average Effective Heat of Combustion, *Avg CO*: Average CO Yield, *Avg CO<sub>2</sub>*: Average CO<sub>2</sub> Yield.

In order to investigate the flame-retardancy mechanism, structural characterization of the char residues of VPE and VPE/FGO composites

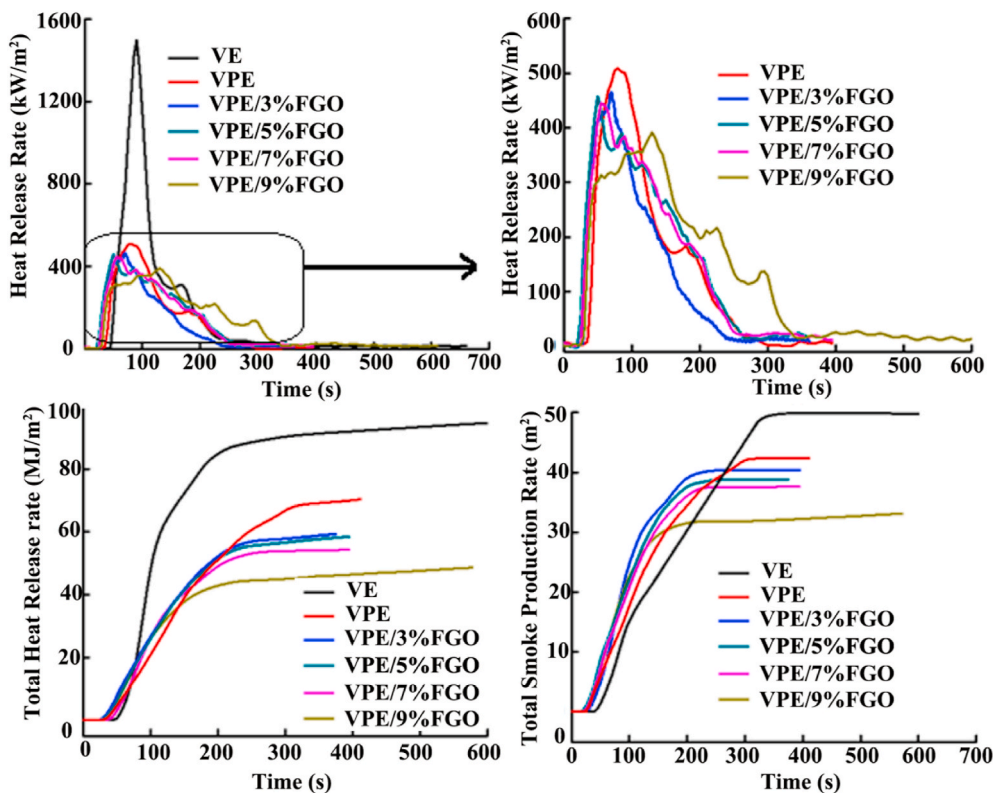


Fig. 8. Cone calorimetry test results (A) Heat Release Rate (HRR) curves, (B) Total Heat Release Rate (THR) curves and (c) Total Smoke Production Rate (TSP) curves.

Table 3

Cone calorimetry data of thermally cured VE, VPE, and VPE/FGO nanocomposites.

Sample Code	Avg HRR (kW/m <sup>2</sup> )	pk HRR (kW/m <sup>2</sup> )	Avg EHC (MJ/kg)	Avg CO (kg/kg)	Avg CO <sub>2</sub> (kg/kg)	Percent Mass Remaining (%)
VE	144.73	1499.00	24.62	0.19	1.87	0.26
VPE	137.68	509.00	12.96	0.17	0.92	5.53
VPE/3% FGO	136.51	465.14	13.47	0.17	0.92	6.10
VPE/5% FGO	132.22	457.46	14.38	0.17	0.89	8.32
VPE/7% FGO	128.13	445.35	14.99	0.16	0.88	9.45
VPE/9% FGO	120.90	391.27	13.01	0.15	0.85	10.93

was performed by FTIR studies, as shown in Fig. 9. These char residues were obtained after the samples were heated in a muffle furnace at 600 °C for 20 min [61]. It was clear that the spectra of all samples showed similar char structures due to their similarity to the spectrum of VPE. For VPE, the broadened peak at 3455 cm<sup>-1</sup> was attributed to the OH group. Vibration absorption peaks at 2954, 2911, and 2848 cm<sup>-1</sup> corresponded to the -CH, -CH<sub>2</sub>, and -CH<sub>3</sub> groups, respectively. The peaks approximately at 1700 cm<sup>-1</sup> revealed that the multi-aromatic structures of the residue char. In addition, the strong absorption peaks at 1260 and 1080 cm<sup>-1</sup> were due to the presence of P-O-P, P-O-Ph and P-N bonds located in the VPE/FGO composites [68]. The decomposition products from phosphate fragmentation and epoxy resins reacted with each other to form cross-linked phosphor carbonaceous and phosphor oxidative char with highly carbonized aromatic networks. The char layer, composed of multi-aromatic carbon and phosphorus containing structures, exhibited high thermal stability, and thus acted as an

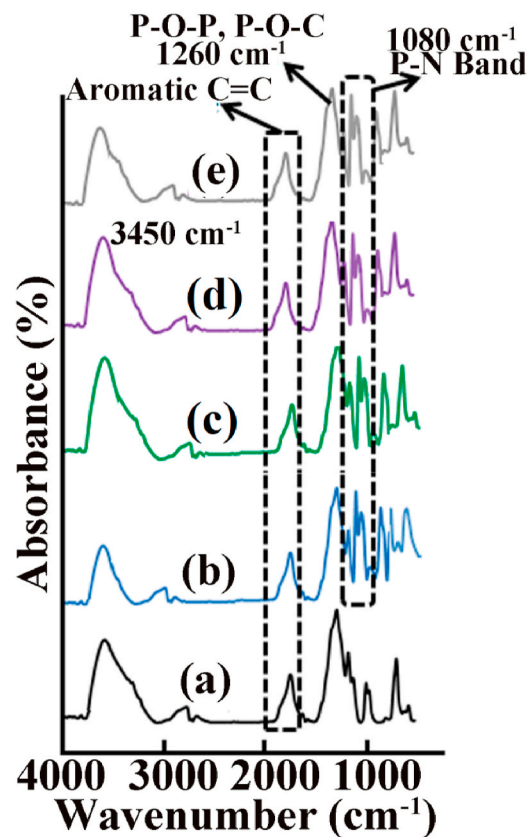


Fig. 9. FTIR spectrum for the char residue of (a) VPE, (b) VPE/3%FGO, (c) VPE/5%FGO, (d) VPE/7%FGO, and (e) VPE/9%FGO.

effective barrier to protect the matrix underneath from decomposing at high temperatures. This study was consistent with the findings from TGA and GC-MS studies.

When compared to the neat VE, VPE and VPE/FGO nanocomposites showed very strong flame-retardant properties by combining two condensed phase flame-retarding strategies, including intumescent flame-retardant mechanism and phosphorus-nitrogen (P–N) synergistic mechanism. The P–N functionalization of GO acted as a char-catalyzing agent to protect graphene from oxygen when burned. This strategy can also be applied as a promising method for improving flame retardancy of polymer systems [69,70].

### 3.9. Conclusion

In this study, we combined bio-based phosphorus containing flame-retardant epoxy resin from vanillin with functionalized GO to make high-performance flame-retardant nanocomposites. FGO was prepared by incorporating phosphorus-nitrogen containing molecule, DDP, onto the surfaces of GO sheets via a non-covalent strategy. The incorporation of FGO accelerated the curing reactions of the resin, indicated that FGO had a catalytic role in reducing the curing time. TGA study showed that even though FGO addition to VPE reduced the earlier decomposition temperature, a significant enhancement effect was found on the char residue caused by the flame-retardant additives catalyzing the degradation of polymers to form the protective char. It was also observed that VPE/FGO nanocomposites showed excellent dry and wet bonding strengths. In addition to the remarkable bonding performance, the VPE/FGO nanocomposites exhibited a superior self-extinguishing flame-retardancy. Especially, VPE/9%FGO sample achieved both the highest LOI value (29.1%) and a UL-94 rating of V-0. From the cone calorimetry test, The HRR, THR, TSP, Avg EHC, Avg CO, and Avg CO<sub>2</sub> of VPE and VPE/FGO nanocomposites were decreased with the increase in the content of FGO compared to those of neat VE. FTIR analysis of the char residues showed an increased intensity of absorption bands of P–O–C, P–O–P, and P–N indicating that P and N elements from FGO retained in the residues. The char layer provided effective shielding to protect the underlying polymers against flame. The approach described herein could be used to develop novel and more efficient graphene-based flame retardants for polymer composite applications. This study demonstrated that the non-covalent functionalization of graphene oxide with flame-retarding compounds provided a novel attractive approach to simultaneously enhance flame retardancy and mechanical strength of the epoxy adhesives.

### CRedit authorship contribution statement

**Pitchaimari Gnanasekar:** Conceptualization, Funding acquisition, Data curation, Formal analysis, Writing - original draft, Conception and design of study, acquisition of data, analysis and/or interpretation of data, Drafting the manuscript. **Heyu Chen:** Funding acquisition, Data curation, Formal analysis, acquisition of data, analysis and/or interpretation of data. **Nicole Tratnik:** Funding acquisition, Data curation, Formal analysis, acquisition of data, analysis and/or interpretation of data. Approval of the version of the manuscript to be published (the names of all authors must be listed). **Martin Feng:** Conceptualization, Conception and design of study, revising the manuscript critically for important intellectual content. **Ning Yan:** Conceptualization, Formal analysis, Data curation, Writing - original draft, Conception and design of study, analysis and/or interpretation of data, Drafting the manuscript, revising the manuscript critically for important intellectual content.

### Declaration of competing interest

The authors declare that they have no known competing financial interests or personal relationships that could have appeared to influence the work reported in this paper.

### Acknowledgement

The authors like to acknowledge financial support from Ontario Centre of Excellence (OCE), Agriculture and Agri-Food Canada (AAFC) VIA-Agri Project #25294, and Natural Science and Engineering Research Council of Canada (NSERC) CRD project #498926.

### Appendix A. Supplementary data

Supplementary data to this article can be found online at <https://doi.org/10.1016/j.compositesb.2020.108585>.

### Associated content

#### Supporting Information

Details of experimental procedures and analytical characterization methods, <sup>1</sup>H, <sup>13</sup>C and <sup>31</sup>P NMR graphs for VP, VE and VPE; Multiple heating rate DSC curves for VE and VPE/3%FGO; Multiple heating rate DSC values for VE, VPE and VPE/FGO nanocomposites; a table for thermal degradation parameters of the cured VE, VPE and FGO/VPE nanocomposites; SEM images of fracture surface of GO, FGO, VPE, and VPE/FGO nanocomposites.

### References

- [1] Tang X, Zhou Y, Peng M. Green preparation of epoxy/graphene oxide nanocomposites using a glycidylamine epoxy resin as the surface modifier and phase transfer agent of graphene oxide. *ACS Appl Mater Interfaces* 2016;8: 1854–66.
- [2] Kumar S, Samal SK, Mohanty S, Nayak SK. Recent development of biobased epoxy resins: a review. *Polym Plast Technol Eng* 2018;57:133–55.
- [3] Pham HHQ, Marks MJ. Epoxy resins in *Ullmann's encyclopaedia of industrial chemistry*. Weinheim 2012;13:155–244.
- [4] Connor JCO, Chapin RE. Critical evaluation of observed adverse effects of endocrine active substances on reproduction and development, the immune system, and the nervous system. *Pure Appl Chem* 2003;75:2099–123.
- [5] Fang F, Huo S, Shen H, Ran S, Wang H, Song P, et al. A bio-based ionic complex with different oxidation states of phosphorus for reducing flammability and smoke release of epoxy resins. *Compos Commun* 2020;17:104–8.
- [6] Guo W, Zhao Y, Wang X, Cai W, Wang J, Song L, et al. Multifunctional epoxy composites with highly flame retardant and effective electromagnetic interference shielding performances. *Compos B Eng* 2020;192:107990.
- [7] Huo S, Yang S, Wang J, Cheng J, Zhang Q, Hu Y, et al. A liquid phosphorus-containing imidazole derivative as flame-retardant curing agent for epoxy resin with enhanced thermal latency, mechanical, and flame-retardant performances. *J Hazard Mater* 2020;386:121984.
- [8] Liu YL. Flame-retardant epoxy resins from novel phosphorus-containing novolac. *Polymer* 2001;42:3445–54.
- [9] Chen H, Chauhan P, Yan N. "Barking" up the right tree: biorefinery from waste stream to cyclic carbonate with immobilization of CO<sub>2</sub> for non-isocyanate polyurethanes. *Green Chem* 2020;22:6874–88.
- [10] Chen H, Nair SS, Chauhan P, Yan N. Lignin containing cellulose nanofibril application in pMDI wood adhesives for drastically improved gap-filling properties with robust bondline interfaces. *Chem Eng J* 2018;360:393–401.
- [11] Wang Z, Gnanasekar P, Nair SS, Farnood R, Yi S, Yan N. Biobased epoxy synthesized from a vanillin derivative and its reinforcement using lignin-containing cellulose nanofibrils. *ACS Sustainable Chem Eng* 2020;8:11215–23.
- [12] Zhang C, Garrison TF, Madbouly SA, Kessler MR. Recent advances in vegetable oil-based polymers and their composites. *Prog Polym Sci* 2017;71:91–143.
- [13] Dai J, Peng Y, Teng N, Liu Y, Liu C, Shen X, et al. High-performing and fire-resistant biobased epoxy resin from renewable sources. *ACS Sustainable Chem Eng* 2018;6:7589–99.
- [14] Maiorana A, Spinella S, Gross RA. Bio-based alternative to the diglycidyl ether of bisphenol A with controlled materials properties. *Biomacromolecules* 2015;16: 1021–31.
- [15] Liu J, Dai J, Wang S, Peng Y, Cao L, Liu X. Facile synthesis of bio-based reactive flame retardant from vanillin and guaiacol for epoxy resin. *Compos B Eng* 2020; 190:107926.
- [16] Aouf C, Lecomte J, Villeneuve P, Dubreucq E, Fulcrand H. Chemo-enzymatic functionalization of gallic and vanillic acids: synthesis of bio-based epoxy resins prepolymers. *Green Chem* 2012;14:2328–36.
- [17] Gnanasekar P, Chen J, Goswami SR, Chen H, Yan N. Sustainable shape-memory polyurethane from abietic acid: superior mechanical properties and shape recovery with tunable transition temperatures. *ChemSusChem* 2020;13:5749–61.
- [18] Hofmann K, Glasser W. Engineering plastics from lignin, 23. Network formation of lignin-based epoxy resins. *Macromol Chem Phys* 1994;195:65–80.

- [19] Zhao J, Dong X, Huang S, Tian X, Song L, Yu Q, et al. "Performance comparison of flame retardant epoxy resins modified by DPO-PHE and DOPO-PHE. *Polym Degrad Stabil* 2018;156:89–99.
- [20] Ma S, Liu X, Jiang Y, Fan L, Feng J, Zhu J. Synthesis and properties of phosphorus-containing bio-based epoxy resin from itaconic acid. *Sci China Chem* 2014;57:379–88.
- [21] Wang S, Ma S, Xu C, Liu Y, Dai J, Wang Z, et al. Vanillin-derived high-performance flame retardant epoxy resins: facile synthesis and properties. *Macromolecules* 2017;50:1892–901.
- [22] Xie W, Tang D, Liu S, Zhao J. Facile synthesis of bio-based phosphorus-containing epoxy resins with excellent flame resistance. *Polym Test* 2020;86:106466.
- [23] Qian XD, Song L, Yu B, Wang B, Yuan B, Shi Y. Novel organic-inorganic flame retardants containing exfoliated graphene: preparation and their performance on the flame retardancy of epoxy resins. *J Mater Chem* 2013;1:6822–30.
- [24] Ran S, Fang F, Guo Z, Song P, Cai Y, Fang Z, et al. Synthesis of decorated graphene with P, N-containing compounds and its flame retardancy and smoke suppression effects on polylactic acid. *Compos B Eng* 2019;170:41–50.
- [25] He W, Song P, Yu B, Fang Z, Wang H. Flame retardant polymeric nanocomposites through the combination of nanomaterials and conventional flame retardants. *Prog Mater Sci* 2020;114:100687.
- [26] Huang G, Huo S, Xu X, Chen W, Jin Y, Li R, et al. Realizing simultaneous improvements in mechanical strength, flame retardancy and smoke suppression of ABS nanocomposites from multifunctional graphene. *Compos B Eng* 2019;177:107377.
- [27] Zhang J, Li Z, Zhang L, García Molleja J, Wang DY. Bimetallic metal-organic framework and graphene oxide nano-hybrids induced carbonaceous reinforcement towards fire retardant epoxy: a novel alternative carbonization mechanism. *Carbon* 2019;153:407–16.
- [28] Zhao H, Ding J, Yu H. Variation of mechanical and thermal properties in sustainable graphene oxide/epoxy composites. *Sci Rep* 2018;8:16560.
- [29] Li J, Zeng X, Ren T, Van der Heide E. The preparation of graphene oxide and its derivatives and their application in bio-tribological systems. *Lubricants* 2014;3:137–61.
- [30] Yan N, Gnanasekar P. Vanillin-derived flame retardant monomers, resins, prepolymers, and polymers, US Patent Application No.63/042,249. June 22, 2020. filed on.
- [31] Gnanasekar P, Feng M, Yan N. Facile synthesis of a phosphorus-containing sustainable biomolecular platform from vanillin for the production of mechanically strong and highly flame-retardant resins. *ACS Sustainable Chem Eng* DOI: 10.1021/acssuschemeng.0c05610.
- [32] Hummers ES, Offeman RE. Preparation of graphitic oxide. *J Am Chem Soc* 1958;80:1339.
- [33] Zaaba NI, Foo KL, Hashim U, Tan SJ, Liu WW, Voon CH. Synthesis of graphene oxide using modified hummers method: solvent influence. *Procedia Engineering* 2017;184:469–77.
- [34] Chen W, Liu P, Min L, Zhou Y, Liu Y, Wang Q, et al. Bi nanoparticles anchored in N-doped porous carbon as anode of high energy density lithium ion battery. *Nano-Micro Lett* 2018;10:39–44.
- [35] Lin CH. Synthesis of novel phosphorus-containing cyanate esters and their curing reaction with epoxy resin. *Polymer* 2004;45:7911–26.
- [36] Gonzalez MG, Baselga J, Cabanelas JC. INTECH Open Access Publisher; 2012.
- [37] Shieh JY, Wang CS. Effect of the organophosphate structure on the physical and flame-retardant properties of an epoxy resin. *J Polym Sci, Part A: Polym Chem* 2002;40:369–78.
- [38] Gaan S, Liang S, Mispreuve H, Perler H, Naescher R, Neisius M. Flame retardant flexible polyurethane foams from novel DOPO-phosphonamide additives. *Polym Degrad Stabil* 2015;113:180–8.
- [39] Ma H, Tong L, Xu Z, Fang Z, Jin Y, Lu F. A novel intumescent flame retardant: synthesis and application in ABS copolymer. *Polym Degrad Stabil* 2007;92:720–6.
- [40] Wu J, Zhang D, Wang Y, Hou B. Electrocatalytic activity of nitrogen-doped graphene synthesized via a one-pot hydrothermal process towards oxygen reduction reaction. *J Power Sources* 2013;227:185–90.
- [41] Ryu SH, Sin Jh Shanmugharaj AM. Study on the effect of hexamethylene diamine functionalized graphene oxide on the curing kinetics of epoxy nanocomposites. *Eur Polym J* 2014;52:88–97.
- [42] Vinnik RM, Roznyatovsky VA. Kinetic method by using calorimetry to mechanism of epoxy-amine cure reaction. *J Therm Anal Calorim* 2003;73:807–17.
- [43] Chhetri S, Samanta P, Murmu NC, Srivastava SK, Kuila T. Electromagnetic interference shielding and thermal properties of non-covalently functionalized reduced graphene oxide/epoxy composites. *AIMS Mater Sci* 2016;4:61–74.
- [44] Fang M, Zhen Z, Li J, Zhang H, Lu H, Yang Y. Constructing hierarchically structured interphases for strong and tough epoxy nanocomposites by amine-rich graphene surfaces. *J Mater Chem* 2010;20:9635–43.
- [45] Jouyandeh M, Yarahmadi E, Didehban K, Ghiyasi S, RezaParan SM, Puglia D, et al. Cure kinetics of epoxy/graphene oxide (GO) nanocomposites: effect of starch functionalization of GO nanosheets. *Prog Org Coating* 2019;136:105217.
- [46] Gnanasekar P, Yan N. Synthesis and thermo-mechanical properties of novel spirobiindane based epoxy nanocomposites with tryptophan as a green hardener: curing kinetics using model free approach. *Polym Degrad Stabil* 2019;163:110–21.
- [47] Jouyandeh M, Yarahmadi E, Didehban K, Ghiyasi S, Paran SMR, Puglia D, et al. Cure kinetics of epoxy/graphene oxide (GO) nanocomposites: effect of starch functionalization of GO nanosheets. *Prog Org Coating* 2019;136:105217.
- [48] Zhang H, Kuila T, Kim NH, Yu DS, Lee JH. Simultaneous reduction, exfoliation, and nitrogen doping of graphene oxide via a hydrothermal reaction for energy storage electrode materials. *Carbon* 2014;69:66–78.
- [49] Kudin KN, Ozbas B, Schniepp HC, Prud'homme RK, Aksay IA, Car R, et al. Spectra of graphite oxide and functionalized graphene sheets. *Nano Lett* 2008;8:36–41.
- [50] Chhetri S, Adak NC, Samanta P, Murmu NC. Kuila T Functionalized reduced graphene oxide/epoxy composites with enhanced mechanical properties and thermal stability. *Polym Test* 2013;63:1–11.
- [51] Wang Y, Shi Z, Yu J, Chen L, Zhu J, Hu Z. Tailoring the characteristics of graphite oxide nanosheets for the production of high-performance poly(vinyl alcohol) composites. *Carbon* 2012;50:5525–36.
- [52] Valles C, David J, Nu N, Benito AM, Maser WK. Flexible conductive graphene paper obtained by direct and gentle annealing of graphene oxide paper. *Carbon* 2012;50:835–44.
- [53] Naem H, Ajmal M, Muntha S, Ambreen J, Siddiq M. Synthesis and characterization of graphene oxide sheets integrated with gold nanoparticles and their applications to adsorptive removal and catalytic reduction of water contaminants. *RSC Adv* 2018;8:3599–610.
- [54] Tang X, Zhou Y, Peng M. Green Preparation of epoxy/graphene oxide nanocomposites using a glycidylamine epoxy resin as the surface modifier and phase transfer agent of graphene oxide. *ACS Appl Mater Interfaces* 2016;8:1854–66.
- [55] Li S, Liu X, Fang C, Liu N, Liu D. Surface modification and thermal performance of a graphene oxide/novolac epoxy composite. *RSC Adv* 2018;8:20505–16.
- [56] Rafiee MA, Rafiee J, Wang Z, Song H, Yu YY, Koratkar N. Enhanced mechanical properties of nano-composites at low graphene content. *ACS Nano* 2009;3:3884–90.
- [57] Li W, Shang T, Yang W, Yang H, Lin S, Jia X, et al. Effectively exerting the reinforcement of dopamine reduced graphene oxide on epoxy-based composites via strengthened interfacial bonding. *ACS Appl Mater Interfaces* 2016;8:13037–50.
- [58] Yu Y, Fu S, Song PA, Luo X, Jin Y, Lu F, et al. Functionalized lignin by grafting phosphorus-nitrogen improves the thermal stability and flame retardancy of polypropylene. *Polym Degrad Stabil* 2012;97:541–6.
- [59] Fang F, Ran S, Fang Z, Song P, Wang H. Improved flame resistance and thermo-mechanical properties of epoxy resin nanocomposites from functionalized graphene oxide *via* self-assembly in water. *Compos B Eng* 2019;165:406–16.
- [60] Guo W, Yu B, Yuan Y, Song L, Hu Y. In situ preparation of reduced graphene oxide/DOPO-based phosphonamide hybrids towards high-performance epoxy nanocomposites. *Compos B Eng* 2017;123:154–64.
- [61] Tian HL, Leu CM, Wei KH. Effect of reactivity of organics-modified montmorillonite on the thermal and mechanical properties of montmorillonite/polyimide nanocomposites. *Chem Mater* 2001;13:222–6.
- [62] Chern YC, Hsieh KH, Hsu JS. Interpenetrating polymer networks of polyurethane cross-linked epoxy and polyurethanes. *J Mater Sci* 1997;32:3503–9.
- [63] Menard R, Negrell-Guirao C, Ferry L, Sonnier R, David G. Synthesis of biobased phosphate flame retardants: characterization of flame retardancy on epoxy thermosets. *Pure Appl Chem* 2014;86:1637–50.
- [64] Zhang W, Li X, Yang R. Blowing-out effect and temperature profile in condensed phase in flame retarding epoxy resins by phosphorus-containing oligomeric silsesquioxane. *Polym Adv Technol* 2013;24:951–61.
- [65] Zhang W, Li X, Yang R. Study on flame retardancy of TGDDM epoxy resins loaded with DOPO-POSS compound and OPS/DOPO mixture. *Polym Degrad Stabil* 2014;99:118–26.
- [66] Luo QQ, Yuan YC, Dong CL. Intumescent flame retardancy of a DGEBA epoxy resin based on 5, 10-dihydro-phenophosphazine-10-oxide. *RSC Adv* 2015;5:68476–84.
- [67] Tai Q, Hu Y, Yuen RKK, Song L, Lu H. Synthesis, structure-property relationships of polyphosphoramides with high char residues. *J Mater Chem* 2011;21:6621–7.
- [68] Potts JR, Dreyer DR, Bielawski CW, Ruoff RS. Graphene-based polymer nanocomposites. *Polymer* 2011;52:5–25.
- [69] Bao CL, Song L, Wilkie CA, Yuan BH, Guo YQ, Hu Y, et al. Graphite oxide, graphene, and metal-loaded graphene for fire safety applications of polystyrene. *J Mater Chem* 2012;22:16399–406.
- [70] Bao CL, Song L, Xing WY, Yuan BH, Wilkie CA, Huang JL, et al. Preparation of graphene by pressurized oxidation and multiplex reduction and its polymer nanocomposites by master batch-based melt blending. *J Mater Chem* 2012;22:6088–96.